Solution Conformation of the (+)-*trans-anti*-[BP]dG Adduct opposite a Deletion Site in a DNA Duplex: Intercalation of the Covalently Attached Benzo[a]pyrene into the Helix with Base Displacement of the Modified Deoxyguanosine into the Major Groove†

Monique Cosman,‡ Radovan Fiala,‡ Brian E. Hingerty,§ Shantu Amin,‖ Nicholas E. Geacintov,⊥ Suse Broyde,# and Dinshaw J. Patel*,‡

Cellular Biochemistry and Biophysics Program, Memorial Sloan-Kettering Cancer Center, New York, New York 10021, Health and Safety Research Division, Oak Ridge National Laboratory, Oak Ridge, Tennessee 37831, American Health Foundation, Valhalla, New York 10595, and Chemistry and Biology Departments, New York University, New York, New York 10003

Received April 27, 1994; Revised Manuscript Received July 28, 1994®

ABSTRACT: This paper reports on the solution structure of the (+)-*trans-anti*-[BP]dG adduct positioned opposite a deletion site in a DNA oligomer duplex which defines the alignment of this covalent benzo[a]pyrene-N^2-deoxyguanosine stereoisomer relative to the deletion site. The combined NMR–molecular mechanics computation studies were undertaken on the (+)-*trans-anti*-[BP]dG adduct embedded in the d(C5-[BP]G6-C7)·d(G16-G17) sequence context in a duplex containing 11 residues on the modified strand and 10 on the partner, with no base opposite the modification. The exchangeable and nonexchangeable protons of the benzo[a]pyrenyl moiety and the nucleic acid were assigned following analysis of two-dimensional NMR data sets in H_2O and D_2O solution. The solution conformation of the (+)-*trans-anti*-[BP]dG·del 11-mer duplex has been determined by incorporating intramolecular and intermolecular proton–proton distances defined by lower and upper bounds deduced from NOESY spectra as restraints in molecular mechanics computations in torsion angle space. The benzo[a]pyrene ring of [BP]dG6 is intercalated between intact Watson–Crick dC5·dG17 and dC7·dG16 base pairs with the deoxyguanosine base of [BP]dG6 displaced into the major groove. The intercalation site is wedge shaped, being narrower toward the dG16-dG17 step on the deletion-containing strand. The deoxyguanosine base of [BP]dG6 which is positioned in the major groove is inclined relative to the helix axis and stacks over the 5′-flanking dC5 residue in the solution structure. The intercalative-base displacement structure of the (+)-*trans-anti*-[BP]dG·del 11-mer duplex exhibits several unusually shifted proton resonances which can be readily accounted for by the ring current contribution of the deoxyguanosyl and pyrenyl rings of the [BP]dG6 adduct. This solution structure of the (+)-*trans-anti*-[BP]dG·del 11-mer duplex where the pyrene ring intercalates into the helix with displacement of the modified deoxyguanosine into the major groove strikingly contrasts with our previous study on the (+)-*trans-anti*-[BP]dG·dC 11-mer duplex [Cosman, M., et al. (1992) *Proc. Natl. Acad. Sci. U.S.A. 89*, 1914–1918] where the benzo[a]pyrene ring is positioned in the minor groove without disruption of the Watson–Crick pairing at the [BP]dG·dC modification site. Thus, generation of the deletion site following removal of the dC opposite the (+)-*trans-anti*-[BP]dG results in a displacement of the entire [BP]dG residue toward the major groove and intercalation of the benzo[a]pyrene ring into the helix.

Polycyclic aromatic hydrocarbons (PAHs), a class of environmental pollutants, are metabolically activated to highly reactive electrophiles which bind to cellular DNA and cause mutations and cancer (Conney, 1982; Harvey, 1991). An important goal in this area of research is the characterization of structure–biological activity relationships and the definition of the critical features of PAH metabolite–DNA adducts which distinguish mutagenic from benign lesions. Benzo[a]pyrene (BP), a representative PAH compound, is metabolized to a number of products [for reviews, see Conney (1982), Singer & Grunberger (1983), and Harvey (1991)], including the highly reactive stereoisomeric 7,8-dihydroxy-9,10-epoxy-7,8,9,10-tetrahydrobenzo[a]pyrene diol epoxides (BPDEs); the two diastereoisomers of BPDE (*anti* and *syn*) can each be resolved into two enantiomers. The extraordinary differences in the mutagenic and tumorigenic activities of the (+) and (−)-*anti*-BPDE enantiomers in bacterial and mammalian cells (Wood et al., 1977; Brookes & Osborne, 1982; Burgess et al., 1985; Stevens et al., 1985; Conney, 1982; Harvey, 1991) render these two stereoisomers of BPDE particularly suitable for detailed DNA adduct structure–biological activity comparisons. The major mode of covalent binding of both enantiomers to DNA involves *cis* and *trans* addition of the exocyclic amino group of the deoxyguanosine residues to the C^{10} position of BPDE (Weinstein et al., 1976; Jeffrey et al., 1976; Koreeda et al., 1978; Meehan & Straub, 1979; Cheng et al., 1989).

The successful large-scale synthesis of BPDE-modified deoxyoligonucleotides containing site-specific and stereochemically specific BP-N^2-dG lesions (Cosman et al., 1990;

† This research was supported by NIH Grant CA-46533 to D.J.P., by NIH Grant CA-20851 and DOE Grant DE-FG02-88ER60405 to N.E.G., by NIH Grant CA-28038, NIH Grant RR-06458, and DOE Grant DE-FG02-90ER60931 to S.B., and by DOE Contract DE-AC05-840R21400 with Martin-Marietta Energy Systems and DOE OHER Field Work Proposal ERKP931 to B.E.H.

* Author to whom correspondence should be addressed.
‡ Memorial Sloan-Kettering Cancer Center.
§ Oak Ridge National Laboratory.
‖ American Health Foundation.
⊥ Chemistry Department, New York University.
Biology Department, New York University.

® Abstract published in *Advance ACS Abstracts,* September 1, 1994.

0006-2960/94/0433-11507$04.50/0

Cosman, 1991; Geacintov et al., 1991) has recently made possible the elucidation of the solution structures of (+)-*trans-anti*-, (−)-*trans-anti*-, and (+)-*cis-anti*-[BP]dG lesions positioned opposite dC in duplex DNA by a combination of high-resolution NMR and computational techniques (Cosman et al., 1992, 1993; de los Santos et al., 1992). The conformations of these three stereoisomeric adducts are strikingly different from one another and could lead to different biological endpoints for each one of these lesions. The (+)-*cis-anti*-[BP]dG lesion is characterized by a base displacement-intercalative conformation (Cosman et al., 1993), while the benzo[a]pyrene is located in the minor groove with the hydrogen bonding alignment of the modified base pair intact in both the (+)-*trans-anti*- and (−)-*trans-anti*-[BP]dG·dC modified duplexes (Cosman et al., 1992; de los Santos et al., 1992).

In site-directed mutagenesis experiments with (+)-*trans-anti*-[BP]dG lesions built into the unique *Pst*I recognition site of the *Escherichia coli*. plasmid pUC19, G to T transversions are observed predominantly (Mackay et al., 1992). Using two different DNA polymerases for studying *in vitro* primer extension reactions (DNA synthesis catalyzed by human polymerase α and Sequenase 2.0), it was found that the (+)-*trans-anti* and (+)-*cis-anti*-[BP]dG lesions strongly block DNA synthesis; only a small amount of fully extended primer oligonucleotides containing dCMP opposite the lesions was observed (Hruszkewcyz et al., 1992). The kinetics of nucleotide insertion opposite the lesions and primer extension past the lesion have been studied in the modified d(---T-C-[BP]G-C-T---) template containing single (+)-*trans-anti*-, (−)-*trans-anti*-, (+)-*cis-anti*-, and (−)-*cis-anti*-[BP]dG lesions catalyzed by the Klenow fragment of *E. coli*. DNA polymerase I. Depending on the stereochemical properties of the lesions, varying amounts of incorporation of dAMP opposite the lesion and one- and two-base deletions were observed (Shibutani et al., 1993). The occurrence of deletions, or frameshift mutations in noniterated sequences containing bulky adducts, suggests that mechanisms involving misaligned template–primer intermediates may be operative (Kunkel, 1990; Schaaper et al., 1990; Shibutani & Grollman, 1993).

Furthermore, UV-melting profiles of duplexes containing single-base deletion sites on the complementary strands opposite [2-acetylaminofluorene-C^8]dG (Garcia et al., 1993) or [BP]dG lesions (Ya et al., 1994) have shown that the presence of the bulky aromatic ring systems increase the thermodynamic stabilities of duplexes containing single-base deletions.

In order to gain a better understanding of the structural basis for deletion mutations, high-resolution two-dimensional NMR techniques, in combination with computational potential energy minimization methods, were used to elucidate the conformation of the (+)-*trans-anti*-[BP]dG residue **1** and (+)-*cis-anti*-[BP]dG residue **2** when positioned opposite a single-base deletion site in the sequence context (C-[BP]G-C)·(G-G) at the 11-mer duplex **3** level. This one-base deletion site constitutes a [BP]dG modified duplex with all bases present on the unmodified complementary strand except for the dC opposite the lesion. This paper reports on the (+)-*trans-anti*-[BP]dG·del 11-mer duplex, and the following paper (Cosman et al., 1994) reports on the (+)-*cis-anti*-[BP]dG·del 11-mer duplex.

MATERIALS AND METHODS

Preparation of the (+)-trans-anti-[BP]dG·del 11-mer Duplex. Racemic *anti*-BPDE was prepared by methods described in the literature (Yagi et al., 1977). The synthesis of the (+)-*trans-anti*-[BP]dG covalent adducts in the d(C-C-A-T-C-[BP]G-C-T-A-C-C) sequence was carried out using previously described methods (Cosman et al., 1990) starting, however, with racemic *anti*-BPDE. The (+)-*trans-anti*-, (−)-*trans-anti*-, (+)-*cis-anti*-, and (−)-*cis-anti*-[BP]dG isomeric covalent adducts at the 11-mer strand level were separable by preparative HPLC on a C18 ODS Hypersil column (Cosman et al., 1990). The modified enantiomerically pure d(C-C-A-T-C-[BP]G-C-T-A-C-C) 11-mer strand was annealed to the complementary unmodified d(G-G-T-A-G-G-A-T-G-G) 10-mer strand at 70 °C, and the stoichiometry was followed by monitoring single proton resonances in both strands.

Chart 1

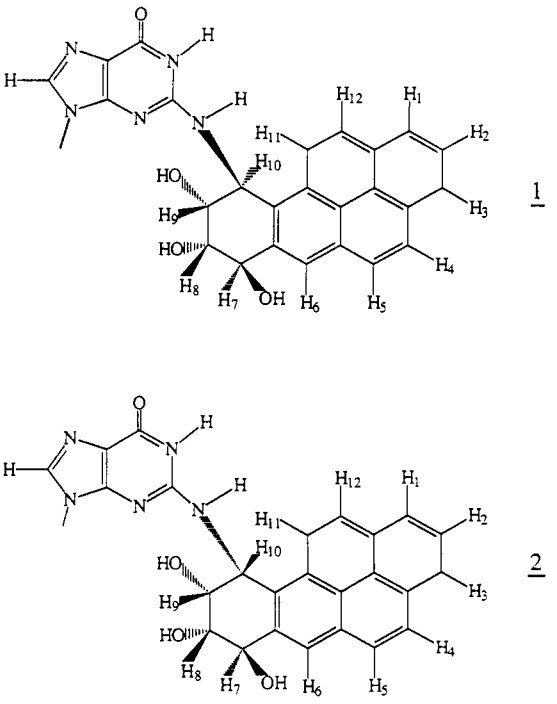

NMR Experiments. A combination of through space nuclear Overhauser enhancement (NOESY) (Kumar et al., 1982) and through-bond correlated (COSY, TOCSY) (Braunschweiler & Ernst, 1983) two-dimensional spectra were recorded and analyzed to assign the benzo[a]pyrene and nucleic acid protons in the (+)-*trans-anti*-[BP]dG·del 11-mer duplex. All experiments were run on Varian Unity and Unity Plus 600-MHz NMR spectrometers in the States-TPPI mode (Marion et al., 1989) with a 2-s relaxation delay between scans. The temperature of the sample was calibrated with an external methanol sample. A NOESY data set (mixing time 150 ms) was recorded on the adduct duplex (~7 mg) in 90% H_2O–10% D_2O buffer (0.6 mL of 0.1 M NaCl, 10 mM phosphate, 0.1 mM EDTA, pH 7.0) at 1 °C using a jump and return pulse sequence. The corresponding data sets on the adduct duplex in D_2O buffer at 20 °C were recorded at mixing times of 50 and 300 ms. Through-bond relay connectivities

in TOCSY data sets were recorded at spin-lock times of 40 and 80 ms in D_2O buffer at 20 °C.

The proton–proton vicinal coupling constants among sugar protons were analyzed from phase-sensitive COSY spectra and used to qualitatively distinguish between the different families of sugar puckers in the (+)-*trans-anti*-[BP]dG·del 11-mer duplex. The relative intensities of the NOE cross peaks between base protons and their own and 5′-flanking sugar H2′, H2″, and H3′ protons were also used to qualitatively distinguish between the A and B family of helices for the modified duplex (van der Ven & Hilbers, 1988). The vicinal proton coupling constants for sugar residues exhibiting unusual phase-sensitive COSY cross peaks were quantitatively determined by simulation of the corresponding cross peaks using the CHORDS program (Majumdar & Hosur, 1992) and updated versions.

Proton–phosphorus correlation spectra on the control (at 25 °C) and adduct (at 20 °C) duplexes in D_2O buffer, pH 7.0, were recorded with indirect detection (Sklenar et al., 1986). Both proton and phosphorus sweep widths were set to 6 ppm with a 1.3-s presaturation of the HDO signal. The phosphorus spectra were referenced relative to external 10% trimethyl phosphate (TMP).

The SPHINX and LINSHA programs (K. Wuthrich, ETH, Zurich) were used to simulate the experimental three-bond couplings for the BP(H7)-BP(H8) and BP(H9)-BP(H10) pairs in the phase-sensitive COSY data sets for the (+)-*trans-anti*-[BP]dG·del 11-mer duplex. The simulations used a modified Karplus relationship that relates the magnitude of the three-bond proton–proton coupling to values of the intervening torsion angle.

Several factors went into the conversion of the NOE intensities into the distance bounds used for the structure determination. The interproton distances were calculated on the basis of the isolated two-spin approximation using the dT(NH3)-dA(H2) fixed distance of 2.92 Å for the NOESY spectrum in H_2O and the dC(H6)-dC(H5) fixed distance of 2.45 Å for the NOESY spectra in D_2O solution. The choice of upper and lower bound ranges for the estimated distances depended on the resolution of the cross peaks in the contour plots. The base proton to sugar H1′ NOE cross peaks in the 50-ms mixing time NOESY data set in D_2O were evaluated to qualitatively differentiate between *syn* (strong NOE) and *anti* (weak NOE) glycosidic torsion angles (Patel et al., 1982).

Molecular Mechanics Computations. Minimized potential energy calculations were carried out with DUPLEX, a molecular mechanics program for nucleic acids that performs potential energy minimizations in the reduced variable domain of torsion angle space (Hingerty et al., 1989). The advantage of torsion space, compared to Cartesian space minimizations, is the vast diminution in the number of variables that must be simultaneously optimized, thereby permitting larger movements from a given starting conformation during minimization, as well as assurance of realistic internal geometry.

DUPLEX uses a potential set similar to the one developed by Olson and co-workers for nucleic acids (Taylor & Olson, 1983), and details have been published previously (Hingerty et al., 1989). We used force field parameters employed previously for the (+)-*trans-anti*-[BP]dG adduct (Hingerty & Broyde, 1985; Singh et al., 1991).

A hydrogen-bond penalty function (Hingerty et al., 1989) was employed in all first-step minimizations to aid the minimizer in locating the Watson–Crick hydrogen-bonded structures indicated by the NMR data. To locate minimum energy conformations with interproton distances available from the experimental NMR data, pseudopotentials (permitting upper and lower bound restraints) were added to the energy, as described previously (Norman et al., 1989; Schlick et al., 1990; Cosman et al., 1992, 1993). Briefly, the following functions were used:

$$F_N = W_N \sum_1^n (d - d_N)^2 \quad (1)$$

$$F_{NN} = W_{NN} \sum_1^n (d - d_{NN})^2 \quad (2)$$

The W's are adjustable weights (in the range of 10–30 kcal/mol·A^2). Weights in this range serve to guide the minimizer toward the structure defined by the NMR data, while permitting the force field, whose predictive capabilities have been demonstrated (Hingerty et al., 1989; Smith et al., 1991) to play its part. d is the current value of the interproton distance, d_N is a target upper bound, and d_{NN} is a target lower bound. Equation 1 is implemented when d is greater than d_N, and equation (2) is implemented when d is less than d_{NN}. The functions are summed over all n target distances. All penalty functions were released in the last minimization steps to yield unrestrained final structures that are energy minima. F_N and F_{NN} can also be used as relative indices of goodness-of-fit to the NMR data. Here the d values are the achieved distances in a given model, and the W's are the weights employed in the search. F_N and F_{NN} are composites, reflecting the overall fit of all the achieved distances to their targets. They both adopt values of zero when all model distances are within the upper and lower NMR distance bounds. Small deviations from the NMR targets, within the uncertainty of the data, are accepted in computed models, and these therefore have nonzero F_N and F_{NN} values. Computations were carried out at the Department of Energy's National Energy Research Supercomputer Center and the National Science Foundation's San Diego Supercomputer Center.

RESULTS

We have measured the thermal transition midpoints at optical concentrations (~10 μM in strands) for the control dG·del 11-mer duplex (t_m = 24 °C) and the (+)-*trans-anti*-[BP]dG·del 11-mer duplex (t_m = 30 °C). The observed stabilization on adduct formation permits us to undertake NMR studies (at millimolar concentrations) on the (+)-*trans-anti*-[BP]dG·del 11-mer duplex at ambient temperature.

Exchangeable Proton Spectra. The exchangeable proton NMR spectrum (10.0–14.0 ppm) of the (+)-*trans-anti*-[BP]-dG·del 11-mer duplex in H_2O buffer, pH 7.0, at 1 °C is plotted in Figure 1A. Three well resolved upfield-shifted imino protons (10.56, 10.96, and 11.05 ppm) are detected in addition to the partially resolved imino protons resonating between 12.7 and 13.7 ppm. These imino protons have been assigned following an analysis of NOE connectivities between them and nearby protons both across the base pair and to flanking base pairs [reviewed in Patel et al. (1987) and van de Ven and Hilbers (1988)].

Expanded regions of the NOESY contour plot (150-ms mixing time) of the adduct duplex in H_2O buffer, pH 7.0, at 1 °C are plotted in Figure 2. The observed NOE patterns establish Watson–Crick pairing at all dG·dC pairs (deoxyguanosine imino to deoxycytidine amino NOE connectivities) and all dA·dT pairs (thymidine imino to deoxyadenosine H2 connectivities) (Figure 2B). We detect imino to imino proton

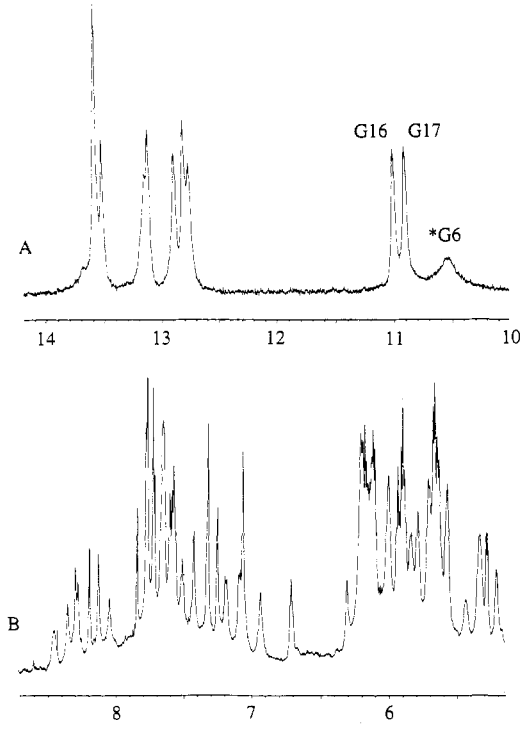

FIGURE 1: (A) Imino proton spectrum (10.0–14.0 ppm) in H_2O buffer at 1 °C and (B) nonexchangeable proton spectrum (5.2–8.7 ppm) in D_2O buffer at 20 °C of the (+)-*trans-anti*-[BP]dG·del 11-mer duplex. The buffer was 0.1 M NaCl, 10 mM phosphate, aqueous solution, pH 7.0. The imino protons of [BP]dG6, dG16, and dG17 are assigned over spectrum A.

NOE connectivities between adjacent nonterminal base pairs on either side of the lesion site (dG12 to dG16 and dG17 to dG20) in the duplex (Figure 2A).

The narrow upfield-shifted imino proton of dG16 (11.05 ppm) flanking the lesion site exhibits NOE cross peaks to the upfield-shifted (5.85 and 6.87 ppm) amino protons of dC7 (peaks A and A′, Figure 2B). Similarly, the narrow upfield-shifted imino proton of dG17 (10.96 ppm) which also flanks the lesion site exhibits NOE cross peaks to the upfield-shifted (5.93 and 7.14 ppm) amino protons of dC5 (peaks B and B′, Figure 2B). These results establish formation of stable dC7·dG16 and dC5·dG17 Watson–Crick base pairs on either side of the [BP]dG6 lesion positioned opposite the deletion site. The observed large upfield shifts of the deoxyguanosine imino and deoxycytidine amino protons for the dC7·dG16 and dC5·dG17 base pairs arise from ring current shifts that must originate from the intercalation of the pyrene ring between these base pairs that flank the [BP]dG6 lesion site.

The broad imino proton at 10.56 ppm is assigned to [BP]-dG6 positioned opposite the deletion site in the adduct duplex. This imino proton exchanges rapidly with solvent, and we do not detect NOEs between it and other protons in the NOESY contour plot in Figure 2. The corresponding amino proton of [BP]dG6 is tentatively assigned to a broad exchangeable resonance at 8.66 ppm. Both the upfield shift and large line width of the imino proton of [BP]dG6 suggest that this deoxyguanosine imino proton positioned opposite the deletion site must be looped out of the helix and exposed to solvent.

The exchangeable imino and amino proton chemical shifts for the central d(C5-[BP]G6-C7)·d(G16-G17) segment of the (+)-*trans-anti*-[BP]dG·del 11-mer duplex at 1 °C are listed in Table 1. The exchangeable proton chemical shift assignments for the entire adduct duplex are listed in Table S1 (Supplementary Material).

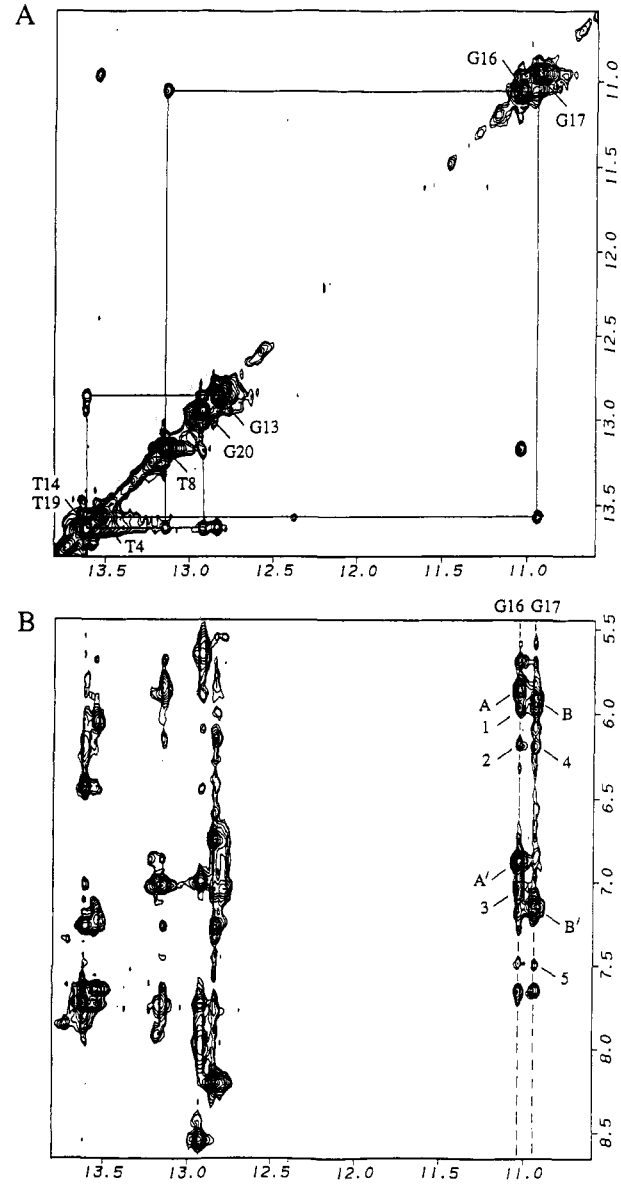

FIGURE 2: Expanded NOESY (150-ms mixing time) contour plots of the (+)-*trans-anti*-[BP]dG·del 11-mer duplex in H_2O buffer, pH 7.0, at 1 °C. (A) NOE connectivities in the symmetrical 10.5–14.0 ppm region. The imino proton assignments are labeled along the diagonal. The lines trace the NOE connectivities between adjacent base pairs starting at dG20 toward one end of the helix and proceeding to dG13 toward the other end of the helix. The imino protons of dG16 and dG17 are separated by a small chemical shift difference. (B) NOE connectivities between the imino protons (10.5–14.0 ppm) and the base and amino protons (5.5–8.5 ppm). The NOE cross peaks involving the imino protons of dG16 and dG17 centered about the lesion site are labeled in the figure. The intramolecular cross peaks A and B between nucleic acid protons are assigned as follows: A,A′, G16(NH1)-C7(NH_2-4b,e); B,B′, G17(NH1)-C5(NH_2-4b,e). The intermolecular cross peaks 1–5 are assigned as follows: (1) G16-(NH1)-BP(H4); (2) G16(NH1)-BP(H5); (3) G16(NH1)-BP(H3); (4) G18(NH1)-BP(H5); (5) G18(NH1)-BP(H2).

Nonexchangeable Nucleic Acid Protons. We observe well resolved nonexchangeable proton spectra (5.2–8.7 ppm) for the (+)-*trans-anti*-[BP]dG·del 11-mer duplex in D_2O buffer at 20 °C (Figure 1B). Nonexchangeable proton assignments were based on an analysis of through-space distance connectivities in NOESY data sets recorded as a function of mixing time and through-bond connectivities in COSY, DQF-COSY, and TOCSY data sets in D_2O buffer at 20 °C.

An expanded 300-ms mixing time NOESY contour plot of the base (6.0–8.5 ppm) and the sugar H1′ and H3′ and

Table 1: Proton Chemical Shifts of the d(C5-[BP]G6-C7)·d(G16-G17) Segment of the (+)-*trans-anti*-[BP]dG·del 11-mer Duplex in Aqueous Buffer

	exchangeable proton chemical shifts (ppm), 1 °C		
	G(NH1)	G(NH_2-2)	C(NH_2-4)
dC5·dG17	10.96		5.93,[b] 7.14[c]
dC7·dG16	11.05		5.85,[b] 6.87[c]
[BP]dG6	10.56	8.66[a]	

	nonexchangeable proton chemical shifts (ppm), 20 °C					
	H8/H6	H2/H5	H1′	H2′,2″	H3′	H4′
dC5	6.13	4.70	5.45	0.94, 1.85	4.34	3.95
[BP]dG6	8.28		6.73	3.21, 2.82	5.35	4.80
dC7	7.67	5.67	5.23	2.01, 2.31	4.45	4.24
dG16	7.61		5.86	2.50, 2.41	5.05	4.48
dG17	8.06		5.64	2.75, 2.83	5.10	4.49

[a] Tentative assignment. [b] Exposed amino proton. [c] Hydrogen-bonded amino proton.

deoxycytidine H5 protons (4.3–6.8 ppm) of the adduct duplex in D_2O buffer at 20 °C is plotted in Figure 3. The base proton (purine H8 or pyrimidine H6) to its own and 5′-flanking sugar H1′ proton connectivities are traced from dT4 to dT8 on the modified strand (full line connectivities in Figure 3) and from dA15 to dA18 on the unmodified strand (dashed line connectivities in Figure 3) for the segment centered about the lesion site. These base and sugar H1′ proton assignments have been confirmed by cross checks in other regions of the NOESY plot which have also yielded a complete set of sugar H2′, H2″, H3′, and H4′ proton assignments for the adduct duplex.

There are several breaks in the connectivities in the chain tracing between the base protons and the sugar H1′ protons as shown for adjacent residue cross peaks which are absent for the dT4-dC5 step and dC5-[BP]dG6 steps on the modified strand and weak for the dG16-dG17 step on the unmodified strand (Figure 3). The connectivities are also perturbed at the [BP]dG6-dC7 step on the modified strand since the NOEs between the base proton of dC7 and the H2′ and H2″ sugar protons of [BP]dG6 are absent and weak, respectively. We also do not detect the characteristic NOE between the H8 proton of [BP]dG6 and the H5 proton of dC7 for the [BP]-dG6-dC7 purine (3′–5′) pyrimidine step in the adduct duplex.

We detect strong NOEs between the H5 proton of dC7 and the H1′ proton of [BP]dG6 and also between the H6 proton of dC7 and the H4′ proton of [BP]dG6 in both 50- and 300-ms mixing time NOESY contour plots. These results require the major groove edge (contains H5 and H6 protons) of the dC7 base to be close to the minor groove face (contains H1′ and H4′ protons) of the sugar ring of [BP]dG6 in the adduct duplex. The H6 (6.13 ppm) and H5 (4.70 ppm) protons of dC5 are shifted dramatically upfield in contrast to the H6 (7.67 ppm) and H5 (5.67 ppm) protons of dC7 which exhibit normal values in the d(C5-[BP]G6-C7) segment of the adduct duplex.

The nonexchangeable proton chemical shifts for the central d(C5-[BP]G6-C7)·d(G16-G17) segment of the (+)-*trans-anti*-[BP]dG·del 11-mer duplex at 20 °C are listed in Table 1. The nonexchangeable proton chemical shift assignments for the entire adduct duplex are listed in Table S2 (Supplementary Material). We have also compared the corresponding exchangeable and nonexchangeable proton shifts between the adduct duplex and the control dG·del 11-mer duplex, and the estimated chemical shift differences are listed in Table S3 (Supplementary Material). The base (H6 and H5) and sugar (H1′, H2′, 2″, H3′ and H4′) protons of dC5 are all shifted

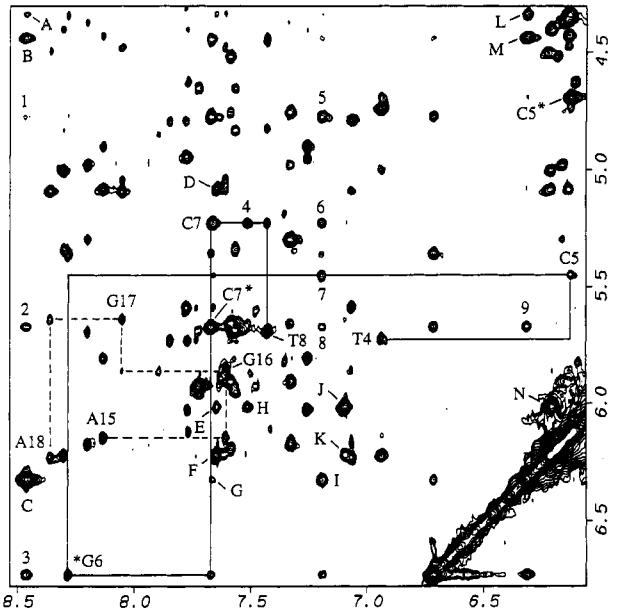

FIGURE 3: Expanded NOESY (300-ms mixing time) contour plot of the (+)-*trans-anti*-[BP]dG·del 11-mer duplex in D_2O buffer at 20 °C establishing distance connectivities between the base (purine H8 and pyrimidine H6) protons (6.0–8.5 ppm) and the sugar H1′ and H3′ and deoxycytidine H5 protons (4.3–6.8 ppm). The NOE connectivities between the base and their own and 5′-flanking sugar H1′ protons from dT4 to dT8 on the modified strand are shown by solid lines and from dA15 to dA18 on the unmodified strand are shown by dashed lines. The assignments label the base to their own sugar H1′ NOEs, while the deoxycytidine H6–H5 NOEs are designated by asterisks. Note the unusual upfield shift of the H6 and H5 protons of dC5 labeled by cross peak C5* and the unusual downfield shift of the H1′ proton of [BP]dG6 labeled by cross peak *G6. Note that the cross peaks linking the dT4-dC5 and dC5-[BP]-dG6 steps are missing while that between dG16 and dG17 is weak. The intramolecular cross peaks A to N between benzo[a]pyrene protons are assigned as follows: (A) BP(H8)-BP(H11); (B) BP-(H9)-BP(H11); (C) BP(H10)-BP(H11); (D) BP(H6)-BP(H7); (E) BP(H4)-BP(H6); (F) BP(H5)-BP(H6); (G) BP(H1)-BP(H10); (H) BP(H2)-BP(H4); (I) BP(H2)-BP(H10); (J) BP(H3)-BP(H4); (K) BP(H3)-BP(H5); (L) BP(H8)-BP(H10); (M) BP(H9)-BP(H10); (N) BP(H4)-BP(H5). The intermolecular cross peaks 1–9 are assigned as follows: (1) G6(H4′)-BP(H11); (2) C7(H5)-BP(H11); (3) G6(H1′)-BP(H11); (4) C7(H1′)-BP(H2); (5) G6(H4′)-BP(H12); (6) C7(H1′)-BP(H12); (7) C5(H1′)-BP(H12); (8) C7(H5)-BP-(H12); (9) C7(H5)-BP(H10). The chemical shift values for the benzylic protons are BP(H7), 5.08 ppm; BP(H8), 4.34 ppm; BP-(H9), 4.44 ppm; BP(H10), 6.32 ppm. The chemical shift values for the pyrenyl protons are BP(H11), 8.46 ppm; BP(H12), 7.19 ppm; BP(H1), 7.66 ppm; BP(H2), 7.51 ppm; BP(H3), 7.09 ppm; BP(H4), 6.01 ppm; BP(H5), 6.21 ppm; BP(H6), 7.65 ppm.

strongly to high field while the base (H8) and sugar (H1′, H2′, H3′, and H4′) protons of [BP]dG6 are shifted to low field on replacement of dG6 by (+)-*trans-anti*-[BP]dG6 adduct in the 11-mer duplex.

The pucker of the sugars in the adduct duplex were probed based on the sugar coupling constant patterns in phase-sensitive COSY spectra and the relative intensities of the NOEs between the base protons and sugar protons in short mixing time NOESY spectra. The dC7 residue exhibits a weak H1′–H2′ coupling (~3 Hz) and strong H2′–H3′, H2″–H3′, and H3′–H4′ couplings (~8 Hz), as well as a strong NOE cross peak between its H6 base and H3′ sugar protons characteristic of a C3′-*endo* sugar pucker. The remaining sugars exhibit coupling constant and NOE patterns characteristic of predominantly C2′-*endo* pucker conformations.

Nonexchangeable Benzo[a]pyrene Protons. The four aliphatic (4.6–6.3 ppm) and eight aromatic (6.0–8.5 ppm) protons of the benzo[a]pyrenyl ring system have been

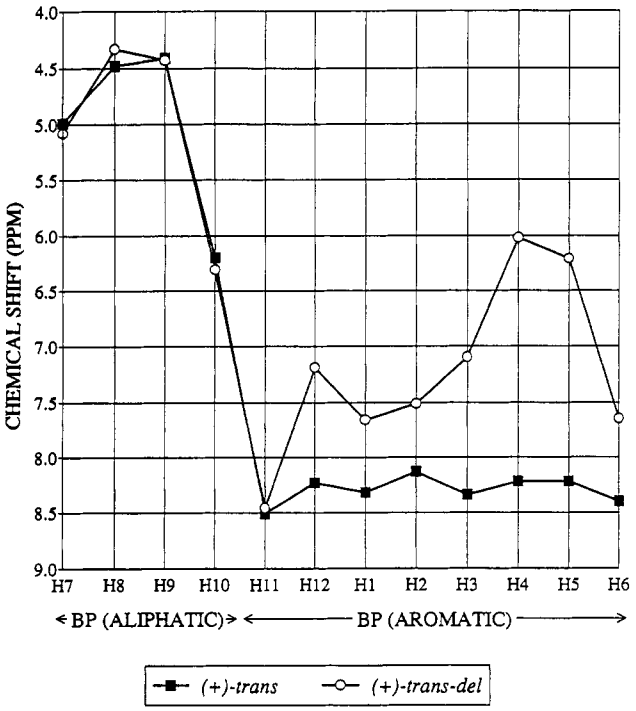

FIGURE 4: Plot comparing the benzo[a]pyrene ring proton chemical shifts in the (+)-*trans-anti*-[BP]dG·dC 11-mer duplex (■) and the (+)-*trans-anti*-[BP]dG·del 11-mer duplex (○). The benzylic protons (H7, H8, H9, H10) are on the left and the pyrenyl (H11, H12, H1, H2, H3, H4, H5, H6) are on the right of this plot. Note the large upfield shifts of the pyrenyl protons on proceeding from the (+)-*trans-anti*-[BP]dG·dC 11-mer duplex to the (+)-*trans-anti*-[BP]-dG·del 11-mer duplex.

completely assigned following analysis of the through-space NOE patterns (Figure 3) and through-bond coupling connectivities in the (+)-*trans-anti*-[BP]dG·del 11-mer duplex. These proton chemical shifts are tabulated in the caption to Figure 3 and plotted in Figure 4.

The pyrenyl ring protons of the benzo[a]pyrene ring should resonate between 8.0 and 8.5 ppm in [BP]dG adducts but are all upfield shifted [except for BP(H11)] in the adduct duplex (Figure 4). The most dramatic upfield shifts are observed for the benzo[a]pyrene H4 and H5 protons.

The experimental coupling cross peaks BP(H7)–BP(H8) and BP(H9)–BP(H10) are well resolved in the phase-sensitive COSY spectrum. We have simulated the coupling cross peak patterns and find that there is good agreement between these experimental cross peak patterns and their simulated counterparts based on three-bond vicinal proton-proton coupling constant values of ^3J(H7,H8) = 8.0 ± 0.5 Hz, ^3J(H8,H9) = 3.0 ± 1.0 Hz, and ^3J(H9,H10) = 3.8 ± 0.8 Hz. These coupling constants restrict the pucker of the benzylic ring to a specific distorted half-chair conformation where the BP(H7) and BP(H8) pair adopt pseudodiaxial conformations (large coupling constants) while the BP(H8) and BP(H9) pair and the BP(H9) and BP(H10) pair adopt pseudodiequatorial orientations (small coupling constants).

Intermolecular NOEs. A set of intermolecular NOEs between nonexchangeable BP protons and exchangeable and nonexchangeable nucleic acid protons have been identified and assigned in the (+)-*trans-anti*-[BP]dG·del 11-mer duplex. Several of these intermolecular NOEs are labeled by numbers in the expanded NOESY contour plot of exchangeable protons in H_2O solution (Figure 2B) and in the expanded NOESY contour plot of nonexchangeable protons in D_2O solution (Figure 3) with the cross peak assignments listed in the figure

Table 2: Comparison of Input Interproton Distance Bounds with Those Observed for the Lowest Energy Solution Structure of the (+)-*trans-anti*-[BP]dG·del 11-mer Duplex

	interproton distances (Å)	
	experimental bounds	observed
exchangeable protons		
C7(NH_2-4h)-BP(H11)	4.0–6.0	4.15
C7(NH_2-4e)-BP(H11)	3.0–5.0	3.94
G16(NH1)-BP(H4)	3.5–5.5	5.32
G16(NH1)-BP(H5)	4.0–6.0	4.57
G17(NH1)-BP(H5)	4.0–6.0	5.51
nonexchangeable protons		
C5(H1′)-BP(H12)	3.5–5.0	4.61
C5(H2′)-BP(H12)	4.5–6.0	5.89
C5(H2″)-BP(H10)	4.5–6.0	6.15
C5(H2″)-BP(H11)	4.5–6.0	4.62
C5(H2″)-BP(H12)	3.5–5.0	4.54
[BP]G6(H1′)-BP(H9)	4.5–6.0	5.81
[BP]G6(H1′)-BP(H10)	3.5–5.0	4.33
[BP]G6(H1′)-BP(H11)	3.5–5.0	3.72
[BP]G6(H1′)-BP(H12)	4.5–6.0	4.45
[BP]G6(H3′)-BP(H12)	4.5–6.0	5.15
[BP]G6(H4′)-BP(H11)	3.0–4.5	3.95
[BP]G6(H4′)-BP(H12)	3.0–4.5	2.71
[BP]G6(H5′H5″)-BP(H12)	3.0–5.5	3.01, 4.01
C7(H1′)-BP(H2)	3.0–5.0	3.41
C7(H1′)-BP(H12)	3.0–5.0	3.30
C7(H5)-BP(H9)	4.0–6.0	5.89
C7(H5)-BP(H10)	3.0–5.0	3.93
C7(H5)-BP(H11)	3.5–5.0	3.66
C7(H5)-BP(H12)	4.0–6.0	4.23
G16(H2′)-BP(H4)	3.5–5.5	5.98
G16(H2″)-BP(H4)	3.5–5.5	4.93

captions. The corresponding intermolecular distance constraints defined by lower and upper bounds for the central d(C5-[BP]G6-C7)·d(G16-G17) segment are listed in Table 2. These 27 intermolecular constraints correspond to resolved NOE cross peaks, while another 13 intermolecular NOEs were identified but were partially overlapped with other cross peaks.

The distribution of nonexchangeable proton distance constraints is such that they are restricted to intermolecular NOEs between the benzo[a]pyrene protons of the carcinogen and the dC5·dG17 and dC7·dG16 base pairs of the nucleic acid (Table 2). A similar observation is made for the distance constraints involving exchangeable protons in that the imino protons of dG16 and dG17 and the amino protons of dC7 exhibit intermolecular NOEs to benzo[a]pyrene protons (Table 2) in the adduct duplex. The combined pattern of specific intermolecular NOEs (Table 2) and upfield proton chemical shifts for nucleic acid (Table S1) and pyrenyl (Figure 4) protons presented above established unambiguously that the benzo[a]pyrene ring which is covalently bonded to the N^2 of dG6 is intercalated between the dC5·dG17 and dC7·dG16 base pairs in the (+)-*trans-anti*-[BP]dG·del 11-mer duplex. We detect nine resolved intermolecular NOEs between the pyrenyl ring protons and the sugar ring protons within the [BP]dG6 residue (Table 2) which provide important constraints for defining the relative alignments of these two components within the lesion modified deoxyguanosine residue in the adduct duplex.

We observe distinct trends in the patterns of intermolecular NOEs for the central d(C5-[BP]G6-C7)·d(G16-G17) segment (Table 2) that permit the alignment of the different edges of the intercalated benzo[a]pyrene ring relative to the modified and unmodified strands of the adduct duplex. Thus, the BP(H10), BP(H11), BP(H12), and BP(H1) protons along one long edge of the benzo[a]pyrene ring exhibit NOEs to the minor groove sugar face of dC5 (H1′ and H2″ protons) and

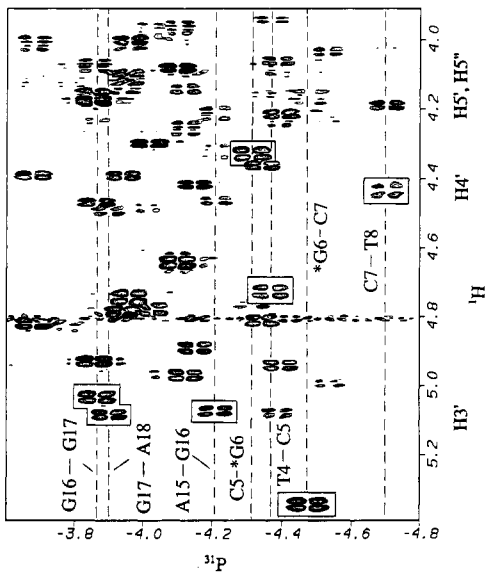

FIGURE 5: Expanded contour plot of the proton-detected phosphorus–proton heteronuclear correlation experiment on the (+)-*trans-anti*-[BP]dG·del 11-mer duplex in D_2O buffer at 20 °C. The phosphorus assignments for steps centered about the lesion site are listed. The correlation cross peaks between the phosphorus and its 5′-linked sugar H3′ protons are boxed.

[BP]dG6 (H1′ and H4′ protons) and NOEs to the major groove base edge of dC7 (H5 and NH_2-4 protons) on the modified strand (Table 2). The BP(H3), BP(H4), BP(H5), and BP(H6) protons located along the other long edge of the benzo[a]pyrene ring exhibit fewer NOEs to DNA protons on the deletion site containing strand in the adduct duplex. Available examples include the intermolecular NOE between the BP(H4) proton and the sugar H2′ and H2″ protons of dG16 and between the BP(H5) proton and the imino protons of dG16 and dG17 that are listed in Table 2.

The benzylic BP(H9) and BP(H10) protons exhibit intermolecular NOEs to the major groove H5 proton of dC7 (Table 2) positioning the benzylic ring of the intercalated benzo[a]pyrene in the major groove of the helix. By contrast, the pyrenyl H2 proton at the other end of the benzo[a]pyrene ring exhibits an intermolecular NOE to the minor groove sugar H1′ proton of dC7 (Table 2) positioning this end of the benzo[a]pyrene ring in the minor groove of the helix. These intermolecular NOEs explicitly establish that the long axis of the intercalated benzo[a]pyrenyl moiety is normal to the long axis of the flanking base pairs and spans both grooves of the helix.

Phosphorus Spectra. The proton-decoupled phosphorus spectrum of the (+)-*trans-anti*-[BP]dG·del 11-mer duplex in D_2O buffer at 20 °C exhibits two downfield shifted and one upfield-shifted phosphorus resonance which are outside the −4.0 to −4.5 ppm spectral region characteristic of unperturbed phosphodiester backbones. The phosphorus resonances have been assigned from an analysis of a proton–phosphorus heteronuclear correlation experiment with the expanded contour plot shown in Figure 5. Each nonterminal phosphorus can be correlated with its 5′-linked H3′ proton and its 3′-linked H4′ and H5′,5″ protons, with the phosphorus resonances assigned on the basis of the known sugar H3′ and H4′ proton assignments. The phosphorus assignments for individual steps in the d(T4-C5-[BP]G6-C7-T8)·d(A15-G16-G17-A18) are listed in Figure 5 with the phosphorus shifts for dG16-dG17 and dG17-dG18 shifted to low field and dC7-dT8 shifted to high field outside the unperturbed range. We have also assigned the phosphorus chemical shifts in the control dG·del 11-mer duplex and plot the chemical shift differences between the control duplex and adduct duplex in Figure S1 (Supplementary Material). We observe upfield shifts (~0.5 ppm) at the dT4-dC5, [BP]dG6-dC7, and dC7-dT8 steps on the modified strand and downfield shifts (~0.4 ppm) at the dG16-dG17 and dG17-dG18 steps on the unmodified strand on proceeding from the control duplex to the adduct duplex (Figure S1).

Molecular Mechanics Computations. Previous computational studies have addressed the alignment of the (+)-*trans-anti*-[BP]dG adduct when embedded in an alternating d(G-C)$_6$·d(G-C)$_6$ duplex (Singh et al., 1991). The approach employed involved conformational searches with potential energy minimization calculations using the molecular mechanics DUPLEX program that operates in torsion angle space (see Materials and Methods) on the dC-[BP]dG and the dC-[BP]dG-dC segments. This was followed by energy-minimized buildup techniques which position the (+)-*trans-anti*-[BP]-dG adduct opposite dC at the DNA oligomer duplex level. These search and build efforts yielded a low energy structure which placed the pyrenyl moiety in the B-DNA minor groove and oriented toward the 5′-direction of the modified strand (Singh et al., 1991). A higher energy structure was also observed in these searches in which the pyrenyl ring was intercalated between flanking dG·dC base pairs resulting in the deoxyguanosine base being displaced into the major groove while the partner deoxycytidine base was displaced into the minor groove (Singh et al., 1991). This structure was used as a starting model for computations on the (+)-*trans-anti*-[BP]dG·del 11-mer duplex system following base sequence adjustment and deletion of the dC residue opposite the [BP]-dG lesion site. This procedure is entirely analogous to the one employed in computing the solution structure of the (+)-*trans-anti*-[BP]dG·dC 11-mer duplex (Cosman et al., 1992) using as a starting model the minor groove conformation of lowest energy (Singh et al., 1991).

The computations were carried out on the central d(T4-C5-[BP]G6-C7-T8)·d(A15-G16-G17-A18) segment with the benzylic ring of [BP]dG6 fixed in the 7,8-diaxial, 9,10-diequatorial conformation as defined by the coupling constant information. The DUPLEX hydrogen bond penalty function (Hingerty et al., 1989) for Watson–Crick pairing was utilized at all base pairs except for the unpaired [BP]dG6 residue, and the computations were guided by the NMR based distance restraints defined by lower and upper bounds which are listed in Table 2.

The starting structure readily converged to its energy-minimized counterpart which satisfied the majority of the experimental distance restraints. The energy of this converged structure was −205 kcal/mol, and goodness-of-fit indices for eqs 1 and 2 were 0.27 and 0.34, respectively, with W = 15 kcal/mol·Å^2. Consequently, the converged structure was embedded in an energy-minimized B-form sequence corresponding to the adduct duplex and reminimized with all experimental restraints. Subsequently, the hydrogen bond penalty function and distance restraints were released with energy minimization in one step, yielding a final unrestrained structure for the (+)-*trans-anti*-[BP]dG·del 11-mer duplex.

Solution Structure. A view normal to the helix axis and looking into the minor groove for the central d(T4-C5-[BP]-G6-C7-T8)·d(A15-G16-G17-A18) segment of the lowest energy NMR-energy minimized structure of the (+)-*trans-anti*-[BP]dG·del 11-mer is shown in Figure 6A. Two views of the structure of the entire adduct duplex are shown in Figure S2 (Supplementary Material). The benzo[a]pyrene moiety

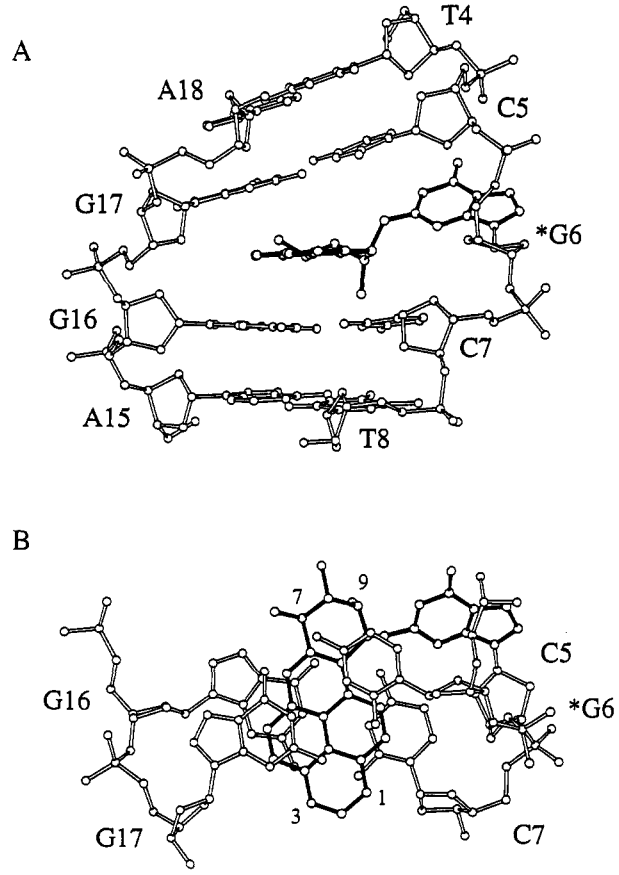

FIGURE 6: (A) View looking into the minor groove and normal to the helix axis for the d(T4-C5-[BP]G6-C7-T8)·d(A15-G16-G17-A18) segment in the solution structure of the (+)-*trans-anti*-[BP]-dG-del 11-mer duplex. The BP ring system is shown in darkened bonds and is intercalated between the dC5·dG17 and dC7·dG16 base pairs which form a wedge-shaped intercalation site. The modified dG6 base is displaced into the major groove, and its plane is tilted by ~140° relative to the helix axis and is directed toward its 5′-neighbor dC5 in the sequence. (B) View looking down the helix axis for the d(C5-[BP]G6-C7)·d(G16-G17) segment in the solution structure of the (+)-*trans-anti*-[BP]dG-del 11-mer duplex. Note that the benzylic ring is positioned toward the major groove, while the pyrenyl ring stacks over the Watson–Crick hydrogen bonding regions of the flanking dC5·dG17 and dC7·dG16 base pairs. The major groove edge of the dC5 sugar ring is positioned over the plane of the displaced modified dG6 residue.

which is covalently linked to the minor groove N^2 of dG6 intercalates between intact Watson–Crick dC5·dG17 and dC7·dG16 base pairs and in the process displaces the deoxyguanosine ring of [BP]dG6 into the major groove (Figure 6A). The major groove face of the sugar ring of dC5 is positioned over the deoxyguanosine base plane of [BP]dG6 which is directed toward the 5′-end of the modified strand and tilted relative to the helix axis. The intercalation site is wedge-shaped resulting in a shorter separation between base planes of dG16 and dG17 on the deletion containing strand relative to base planes of dC5 and dC7 on the modified strand (Figure 6A).

The long axis of the intercalated benzo[a]pyrenyl ring is normal to the long axis of the flanking dC5·dG17 and dC7·dG16 base pairs with its benzylic ring positioned in the major groove and the farthest aromatic ring on the pyrene extending into the minor groove (Figure 6B). This intercalation orientation positions the pyrene ring directly over the Watson–Crick edge of both flanking dG·dC base pairs (Figure 6B).

The benzylic ring of BP retains a distorted half-chair conformation with the BP(H7) and BP(H8) in pseudodiaxial orientations while the BP(H9) and BP(H10) protons adopt pseudodiequatorial orientations (Neidle et al., 1982). The carcinogen-base linkage site for the [BP]dG6 residue is defined by the angles α'[dG6(N^1)-dG6(C^2)-dG6(N^2)-BP(C^{10})] = 138° and β'[dG6(C^2)-dG6(N^2)-BP(C^{10})-BP(C^9)] = 263° in the NMR energy-minimized structure of the (+)-*trans-anti*-[BP]dG·del 11-mer duplex.

The glycosidic torsion angles, sugar puckers and backbone torsion angles for the d(T4-C5-[BP]G6-C7-T8)·d(A15-G16-G17-A18) segment of the (+)-*trans-anti*-[BP]dG·del 11-mer duplex are listed in Table S4 (Supplementary Material). The glycosidic χ angle for [BP]dG6 (301°) is in the high *anti* range compared to values between 220° and 240° for the remaining residues in the central segment (Table S4). The pseudorotation parameter **P** value for dC7 (15°) is in the C3′-*endo* range compared to values between 150° and 170° (C2′-*endo*) for the remaining residues except for dG16 whose **P** value is 92°. The ζ backbone torsion angle of 111° for the [BP]dG6-dC7 step is distinct from values in the 245° to 290° range for the remaining residues in the central segment.

Convergence to very similar final structures resulted when the lowest energy NMR energy-minimized structure was distorted by +45° or −45° at each of the two bonds (α' and β') at the base-carcinogen linkage and reminimized with restraints. Two views of the best-fit superposition of the resulting four structures are plotted in Figure S3 (Supplementary Material).

DISCUSSION

Spectral Quality. The exchangeable imino (Figure 1A) and nonexchangeable (Figure 1B) proton resonances are well resolved for the (+)-*trans-anti*-[BP]dG·del 11-mer duplex. The proton resonances from the central d(T4-C5-[BP]G6-C7-T8)·d(A15-G16-G17-A18) segment are especially well resolved as can be seen by the upfield-shifted imino protons of [BP]dG6, dG16, and dG17 in Figure 1A. The (+)-*trans-anti*-[BP]dG·del 11-mer duplex adopts a single conformation on the basis of the proton spectra (Figure 1) and the absence of exchange cross peaks in the NOESY spectra.

The solution structure of the central segment of the (+)-*trans-anti*-[BP]dG·del 11-mer duplex shown in Figure 6 establishes that the covalently attached benzo[a]pyrene ring intercalates between intact Watson–Crick dC5·dG17 and dC7·dG16 base pairs with the deoxyguanosine ring of [BP]-dG6 positioned in the major groove and inclined relative to the helix axis. This unusual alignment of [BP]dG6 combined with the intercalation of the benzo[a]pyrene ring should result in a set of novel NOE and chemical shift patterns distinct from unperturbed helices. This structure must not only satisfy the distance restraints but also be consistent with the observed chemical shift changes associated with intercalation of the pyrene ring into the helix.

NOE Patterns. The orientation of the intercalated benzo-[a]pyrene ring between the flanking dG·dC base pairs in the solution structure of the (+)-*trans-anti*-[BP]dG·del 11-mer duplex (Figure 6B) is supported by both the experimental NOE and chemical shift data. Thus, alignment of the C^{10}-C^{11}-C^{12} containing long edge of the BP ring toward the d(C5-[BP]G6-C7) segment of the modified strand (Figure 6B) results in the observation of intermolecular NOEs between the BP(H10), BP(H11), and BP(H12) protons and the sugar protons of dC5, [BP]dG6, and dC7 which are satisfied in the solution structure (Table 2). The BP(H11) and BP(H12) protons are primarily stacked over dC7 in the solution structure (Figure 6B) consistent with the observed intermolecular NOEs

between these BP protons and the NH_2-4 and H5 base protons of dC7 (Table 2). The alignment of the C^4-C^5-C^6 containing edge of the BP ring toward the d(G16-G17) segment of the deletion containing strand (Figure 6B) results in intermolecular NOEs between the BP(H5) and BP(H6) protons with the imino and sugar protons of dG16 and dG17 which are satisfied in the solution structure (Table 2). The C^1-C^2-C^3 edge of the pyrenyl ring is positioned in the minor groove while the C^7-C^8-C^9 edge of the benzylic ring of BP is positioned in the major groove in the solution structure of the (+)-*trans-anti*-[BP]dG·del 11-mer duplex (Figure 6B). We observe only a few intermolecular NOEs involving the protons on these edges of the BP ring (Table 2) consistent with these BP protons being farthest from both strands of the DNA duplex (Figure 6B).

The base displacement of the deoxyguanosine of [BP]dG6 into the major groove in the solution structure of the (+)-*trans-anti*-[BP]dG·del 11-mer duplex should result in unusual NOE patterns for the d(C5-[BP]G6-C7)·d(G16-G17) segment centered about the lesion site. A listing of key NOEs between DNA protons on adjacent residues for this segment are listed as strong, weak, very weak, and absent in Table S5 (Supplementary Material) and can be compared with the corresponding distances measured in the deduced solution structure. The sequential NOE connectivity between the H8 proton of [BP]dG6 and the H1′ proton of dC5 is absent for the dC5-[BP]dG6 step (Figure 3) consistent with the observed distance of 5.91 Å between these protons in the solution structure. The strong NOEs between the H5 proton of dC7 and the H1′ proton of [BP]dG6 and between the H6 proton of dC7 and the H4′ proton of [BP]dG6 observed experimentally for the [BP]dG6-dC7 step are satisfied by the short distances (2.74 and 2.26 Å, respectively) between these proton pairs in the deduced solution structure (Table S5). Similarly, the weak NOE from the H6 proton of dC7 to the H1′ proton of [BP]dG6 for the same step is matched by the 3.76 Å distance between these two protons in the deduced solution structure (Table S5). Finally, the 6.21 Å distance between the H8 proton of [BP]dG6 and the H5 proton of dC7 in the solution structure is consistent with the absence of an NOE between these base protons for this purine (3′–5′) pyrimidine step in the NOESY spectrum of the adduct duplex (Table S5).

The wedge-shaped alignment of the dG16-dG17 step associated with positioning the deletion site opposite the (+)-*trans-anti*-[BP]dG6 adduct also results in a pattern of NOEs that are satisfied by the solution structure. The 6.08 Å distance between the H8 protons of dG16 and dG17 observed in the solution structure is consistent with the absence of an NOE between these protons in the experimental data (Table S5). The NOEs between the H8 proton of dG17 and the H1′ and H3′ protons of dG16 range from very weak to weak consistent with distances of 5.23 and 4.44 Å, respectively, separating these proton pairs in the solution structure (Table S5).

Chemical Shift Patterns. Intercalation of the pyrene ring between the dC7·dG16 and dC5·dG17 base pairs in the solution structure of the (+)-*trans-anti*-[BP]dG·del 11-mer duplex (Figure 6) should result in dramatic chemical shift changes for both benzo[a]pyrene and nucleic acid protons. The long axis of the pyrenyl ring is orthogonal to the long axis of the flanking dG·dC base pairs in the solution structure of the adduct duplex with the pyrene ring roughly equidistant from both strands and spanning both the minor and major grooves of the helix (Figure 6). Experimentally, large upfield shifts are detected at the imino protons of dG16 (–1.71 ppm) and dG17 (–1.59 ppm) and the amino protons of dC5 (–0.97, –1.21 ppm) and dC7 (–0.88, –1.07 ppm) on proceeding from the control duplex (contains dG6 instead of [BP]dG6) to the adduct duplex (Table S3). These upfield shifts are readily assigned to ring current contributions of the pyrenyl ring since the imino protons of dG16 and dG17 and the amino protons of dC5 and dC7 are positioned over the pyrene ring in the solution structure of the adduct duplex (Figure 6B). We also note that the pyrenyl ring protons (H12, H1, H2, H3, H4, H5, and H6) are upfield shifted in the (+)-*trans-anti*-[BP]-dG·del 11-mer duplex where the pyrenyl ring intercalates into the helix (this study), in contrast to their values in the (+)-*trans-anti*-[BP]dG·dC 11-mer duplex where the pyrenyl ring is positioned in the minor groove (Cosman et al., 1992) (Figure 4). This reflects upfield ring current shifts at the intercalated pyrenyl protons from the flanking dG·dC base pairs for deletion site adduct containing duplex, with the most pronounced upfield shift observed at the BP(H4) and BP(H5) protons (Figure 4) which are positioned over the purine rings of dG16 and dG17 in the solution structure (Figure 6B).

The dC5 residue is positioned over the deoxyguanosine ring plane of [BP]dG6 which has been displaced into the major groove in the solution structure of the adduct duplex (Figure 6A). This alignment readily explains the large upfield shifts observed experimentally at the H6 (–1.24 ppm), H5 (–0.92 ppm), H1′ (–0.48 ppm), H2′,2″ (–1.03, –0.40 ppm), H3′ (–0.61 ppm), and H4′ (–0.15 ppm) protons of dC5 on proceeding from the control duplex to the structure of the adduct duplex (Table S3). The displacement of the deoxyguanosine ring of [BP]dG6 out of the helix in the solution structure of the adduct duplex explains the trend in the downfield shifts observed at the H8 (+0.41 ppm), H1′ (+0.80 ppm), H2′,2″ (+0.66, +0.27 ppm), H3′ (+0.36 ppm), and H4′ (+0.47 ppm) protons of [BP]dG6 on proceeding from the control duplex to the adduct duplex (Table S3).

Comparison of (+)-trans-anti-[BP]dG Adduct Opposite dC and Deletion Site. The solution structure of the central segment of the (+)-*trans-anti*-[BP]dG·dC 11-mer duplex (Cosman et al., 1992) and the (+)-*trans-anti*-[BP]dG·del 11-mer duplex (this study) are shown in the same relative global orientation of the DNA in Figure 7, panels A and B, respectively. We note that the orientation of the [BP]dG6 residue is strikingly different in the two structures with the benzo[a]pyrene ring positioned in the minor groove without base pair disruption and directed toward the 5′-end of the modified strand when the adduct is positioned opposite dC (Figure 7A) and intercalated into the helix with displacement of the modified deoxyguanosine into the major groove when the adduct is positioned opposite a deletion site (Figure 7B). Further, one face of the benzo[a]pyrene ring is exposed to solvent in the [BP]dG·dC structure (Figure 7A) while the benzo[a]pyrene ring is intercalated between base pairs in the [BP]dG·del structure (Figure 7B). Thus, replacement of the partner deoxycytosine by a deletion site opposite the (+)-*trans-anti*-[BP]dG adduct results in a dramatic conformational transition where both the modified deoxyguanosine base and the attached benzo[a]pyrene ring system are displaced in the direction of the major groove.

We note that the (+)-*trans-anti*-[BP]dG residue prefers to pair with its partner dC through Watson–Crick [BP]dG·dC alignment (Figure 7A) but intercalates the benzo[a]pyrene ring rather than the modified deoxyguanosine into the helix when the [BP]dG residue lacks a pairing partner as in the present case where it is positioned opposite a deletion site (Figure 7B). These results suggest that hydrophobic carcinogen base-stacking interactions between the aromatic

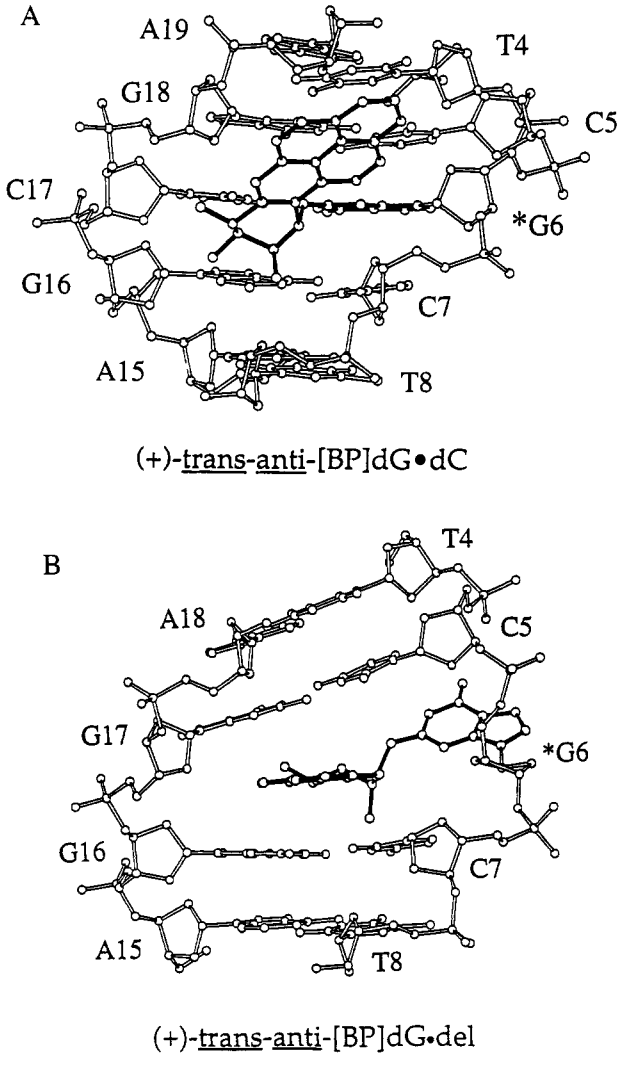

FIGURE 7: Views looking into the minor groove and normal to the helix axis for the solution structures of (A) the d(T4-C5-[BP]G6-C7-T8)·d(A15-G16-C17-G18-A19) segment of the (+)-*trans-anti*-[BP]dG·dC 11-mer duplex and (B) the d(T4-C5-[BP]G6-C7-T8)·d(A15-G16-G17-A18) segment of the (+)-*trans-anti*-[BP]dG·del 11-mer duplex. The orientation of the DNA is similar in the two structures with the BP ring positioned in the minor groove without disruption of the [BP]dG6·dC17 base pair in panel A and the BP ring intercalated into the helix with displacement of the modified dG6 base into the major groove in panel B.

pyrenyl ring system and neighboring base pairs constitutes an important factor in the conformation of this deletion structure.

Strand Slippage and Adduct Conformation. Streisinger et al. (1966) proposed that "slipped mispairing" in repetitive sequences of bases can give rise to deletion or frameshift mutations. Such a mutation mechanism could occur in the case of unmodified DNA (Bebenek & Kunkel, 1990) or in damaged DNA containing a carcinogen-modified base embedded in iterated (Kunkel, 1990; Lambert et al., 1992; Napolitano et al., 1994) and in noniterated base sequences (Kunkel, 1990; Schaaper et al., 1990; Shibutani & Grollman, 1993). In the case of noniterated sequences containing one single carcinogen-modified base (lesion), the polymerases would first incorporate an incorrect base opposite the lesion on the nascent primer strand. Polymerases are known to stall at such adduct sites, which would allow for the formation of misaligned primer-template intermediates. If the incorrect base inserted opposite the lesion is complementary to the base flanking the lesion on the 5′-side of the template strand, a prolonged stalling of the polymerase could give rise to misaligned primer-template intermediates (strand slippage), in which the misincorporated base pairs with the 5′-flanking base on the template strand. Subsequent elongation would fix the misaligned primer-template strand with the carcinogen-modified base in a bulged conformation, resulting in a −1 base deletion mutation (Kunkel, 1990). The results of this study provide unique insights, based on experimental data, into the conformational characteristics of a bulky polycyclic residue at a single-base deletion site which represent the view following mutagenic replication.

SUPPLEMENTARY MATERIAL AVAILABLE

Five tables listing exchangeable proton and nonexchangeable proton chemical shifts, proton chemical shift differences on adduct formation, backbone torsion angles of the lowest energy structure for the central trinucleotide segment, and a comparison of intramolecular nucleic acid proton–proton separations with the corresponding magnitude of experimental NOEs for the adduct duplex, and three figures showing the phosphorus chemical shifts on adduct formation, two views of the entire adduct duplex, and superposition of four structures derived following energy minimization with constraints from the lowest energy structure in which the α' and β' angles were changed by ±45° (10 pages). Ordering information is given on any current masthead page.

REFERENCES

Bebenek, K., & Kunkel, T. A. (1990) *Proc. Natl. Acad. Sci. U.S.A. 87*, 4946–4950.

Braunschweiler, L., Ernst, R. R., & Wüthrich, K. (1983) *J. Magn. Reson. 53*, 521–528.

Brookes, P., & Osborne, M. R. (1982) *Carcinogenesis 3*, 1223–1226.

Burgess, J. A., Stevens, C. W., & Fahl, W. E. (1985) *Cancer Res. 45*, 4257–4262.

Cheng, S. C., Hilton, B. D., Roman, J. M., & Dipple, A. (1989) *Chem. Res. Toxicol. 2*, 334–340.

Conney, A. H. (1982) *Cancer Res. 42*, 4875–4917.

Cosman, M. (1991) Ph.D. Dissertation, New York University, New York.

Cosman, M., Ibanez, V., Geacintov, N. E., & Harvey, R. G. (1990) *Carcinogenesis 11*, 1667–1672.

Cosman, M., de los Santos, C., Fiala, R., Hingerty, B. E., Singh, S. B., Ibanez, V., Margulis, L. A., Live, D., Geacintov, N. E., Broyde, S., & Patel, D. J. (1992) *Proc. Natl. Acad. Sci. U.S.A. 89*, 1914–1918.

Cosman, M., de los Santos, C., Fiala, R., Hingerty, B. E., Luna, E., Harvey, R. G., Geacintov, N. E., Broyde, S., & Patel, D. J. (1993) *Biochemistry 32*, 4145–4155.

Cosman, M., Fiala, R., Hingerty, B. E., Amin, S., Geacintov, N. E., Broyde, S., & Patel, D. J. (1994) *Biochemistry* (following paper in this issue).

de los Santos, C., Cosman, M., Hingerty, B. E., Ibanez, V., Margulis, L. A., Geacintov, N. E., Broyde, S., & Patel, D. J. (1992) *Biochemistry 31*, 5245–5252.

Garcia, A., Lambert, I. B., & Fuchs, R. P. P. (1993) *Proc. Natl. Acad. Sci. U.S.A. 90*, 5989–5993.

Geacintov, N. E., Cosman, M., Mao, B., Alfano, A., Ibanez, V., & Harvey, R. G. (1991) *Carcinogenesis 12*, 2099–2108.

Harvey, R. G. (1991) *Polycyclic Aromatic Hydrocarbons: Chemistry and Carcinogenicity*, Cambridge University Press.

Hingerty, B. E., & Broyde, S. (1985) *Biopolymers 24*, 2279–2299.

Hingerty, B. E., Figueroa, S., Hayden, T., & Broyde, S. (1989) *Biopolymers 28*, 1195–1222.

Hruszkewycz, A. M., Canella, K. A., Peltonen, K., Kotrappa, L., & Dipple, A. (1992) *Carcinogenesis 13*, 2347–2352.

Jeffrey, A. M., Jennette, K. W., Blobstein, S. H., Weinstein, I. B., Beland, F. A., Harvey, R. G., Kasai, H., Miura, I., & Nakanishi, K. (1976) *J. Am. Chem. Soc. 98*, 5714–5715.

Koreeda, M., Moore, P. D., Wistocki, P. G., Levin, W., Conney, A. H., Yagi, H., & Jerina, D. M. (1978) *Science 199*, 778–781.

Kumar, A., Ernst, R. R., Wüthrich, K. (1980) *Biochem. Biophys. Res. Commun. 95*, 1–6.

Kunkel, T. A. (1990) *Biochemistry 29*, 8003–8011.

Lambert, I. B., Napolitano, R. L., & Fuchs, R. P. (1992) *Proc. Natl. Acad. Sci. U.S.A. 89*, 1310–1314.

Mackay, W., Benasutti, M., Drouin, E., & Loecher, E. L. (1992) *Carcinogenesis 13*, 1415–1425.

Majumdar, A., & Hosur, R. V. (1992) *Progr. Nucl. Magn. Reson. Spectrosc. 24*, 109–158.

Marion, D., Ikura, M., Tschudin, R., & Bax, A. (1989) *J. Magn. Reson. 85*, 393–399.

Meehan, T., & Straub, K. (1979) *Nature 277*, 410–412.

Napolitano, R. L., Lambert, I. P., & Fuchs, R. P. (1994) *Biochemistry 33*, 1311–1315.

Neidle, S., Subiah, A., Kuroda, R., & Cooper, C. S. (1982) *Cancer Res. 42*, 3766–3768.

Norman, D., Abuaf, P., Hingerty, B. E., Live, D., Grunberger, D., Broyde, S., & Patel, D. J. (1989) *Biochemistry 28*, 7462–7476.

Patel, D. J., Kozlowski, S. A., Nordheim, A., & Rich, A. (1982) *Proc. Natl. Acad. Sci. U.S.A. 79*, 1413–1417.

Patel, D. J., Shapiro, L., & Hare, D. (1987) *Annu. Rev. Biophys. Biophys. Chem. 16*, 423–454.

Schaaper, R. M., Koffel-Schwarz, N., & Fuchs, R. P. (1990) *Carcinogenesis 11*, 1087–1095.

Schlick, T., Hingerty, B. E., Peskin, C. S., Overton, M. L., & Broyde, S. (1990) in *Theoretical Chemistry and Molecular Biophysics* (Beveridge, D., Live, D., & Lavery, R., Eds.) pp 39–58, Academic Press, New York.

Shibutani, S., & Grollman, A. P. (1993) *J. Biol. Chem. 268*, 11703–11710.

Shibutani, S., Margulis, L. A., Geacintov, N. E., & Grollman, A. P. (1993) *Biochemistry 32*, 7531–7541.

Singer, B., & Grunberger, D. (1983) *Molecular Biology of Mutagens and Carcinogens*, Plenum Press, New York.

Singh, S. S., Hingerty, B. E., Singh, U. C., Greenberg, J. P., Geacintov, N. E., & Broyde, S. (1991) *Cancer Res. 51*, 3482–3492.

Sklenar, V., Miyashiro, H., Zon, G., Miles, H. T., & Bax, A. (1986) *FEBS Lett. 208*, 94–98.

Stevens, C. W., Bouck, N., Burgess, J. A., & Fahl, W. E. (1985) *Mutat. Res. 152*, 5–14.

Streisinger, G., Okada, Y., Emrich, J., Newton, J., Tsugita, A., Terzaghi, E., & Inouye, M. (1966) *Cold Spring Harbor Symp. Quant. Biol. 31*, 77–84.

Taylor, E. R., & Olson, W. K. (1983) *Biopolymers 22*, 2667–2702.

van de Ven, F. J., & Hilbers, C. W. (1988) *Eur. J. Biochem. 178*, 1–38.

Weinstein, I. B., Jeffrey, A. M., Jennette, K. W., Blobstein, S. H., Harvey, R. G., Harris, C., Autrup, H., Kasai, H., & Nakanishi, K. (1976) *Science 193*, 592–594.

Wood, A. W., Chang, R. L., Levin, W., Yagi, H., Thakker, D. R., Jerina, D. M., & Conney, A. H. (1977) *Biochem. Biophys. Res. Commun. 77*, 1389–1396.

Ya, N. Q., Smirnov, S., Cosman, M., Bhanot, S., Ibanez, V., & Geacintov, N. E. (1994) *Proceedings Eighth Conversation Biomolecular Stereodynamics* Sarma, R. H., & Sarma, M. H., Eds.) pp 349–366, Adenine Press, Schenectady, New York.

Yagi, H., Thakker, D. R., Hernandez, O., Koreeda, M., & Jerina, D. M. (1977) *J. Am. Chem. Soc. 99*, 1604–1611.